Published in final edited form as:
Nat Commun. 2013 ; 4: 2535. doi:10.1038/ncomms3535.

Miz1 is required to maintain autophagic flux

Elmar Wolf[1], **Anneli Gebhardt**[1], **Daisuke Kawauchi**[2], **Susanne Walz**[1], **Björn von Eyss**[1], **Nicole Wagner**[3], **Christoph Renninger**[3], **Georg Krohne**[1], **Esther Asan**[3], **Martine F. Roussel**[2], and **Martin Eilers**[1,4,6]

[1] Theodor Boveri Institute, Biocenter, University of Würzburg, Am Hubland, 97074 Würzburg, Germany

[2] Department of Tumor Cell Biology, MS#350, Danny Thomas Research Center, 5006C, St. Jude Children's Research Hospital, Memphis, Tennessee, 38105, USA

[3] Institute for Anatomy and Cell Biology, University of Würzburg, Koellikerstr. 6, 97070 Würzburg, Germany

[4] Comprehensive Cancer Center Mainfranken, Josef-Schneider-Str.6, 97080 Würzburg, Germany

Abstract

Miz1 is a zinc finger protein that regulates expression of cell cycle inhibitors as part of a complex with Myc. Cell cycle-independent functions of Miz1 are poorly understood. Here, we use a Nestin-Cre transgene to delete an essential domain of Miz1 in the central nervous system (*Miz1*$^{\Delta POZNes}$). *Miz1*$^{\Delta POZNes}$ mice display cerebellar neurodegeneration characterized by the progressive loss of Purkinje cells. Chromatin immunoprecipitation (ChIP)-sequencing and biochemical analyses show that Miz1 activates transcription upon binding to a non-palindromic sequence present in core promoters. Target genes of Miz1 encode regulators of autophagy and proteins involved in vesicular transport that are required for autophagy. Miz1$^{\Delta POZ}$ neuronal progenitors and fibroblasts show reduced autophagic flux. Consistently, polyubiquitinated proteins and p62/Sqtm1 accumulate in cerebella of *Miz1*$^{\Delta POZNes}$ mice, characteristic features of defective autophagy. Our data suggest that Miz1 may link cell growth and ribosome biogenesis to the transcriptional regulation of vesicular transport and autophagy.

Introduction

The POZ (Pox virus and Zinc finger)-domain/zinc finger protein Miz1 was first identified as a partner protein of Myc and forms a ternary complex with Myc and Max on DNA. Myc/Miz1 complexes block transcription of their target genes in response to specific anti-mitogenic signals: for example, Myc and Miz1 inhibit activation of the cell cycle inhibitor

[6] Corresponding author martin.eilers@biozentrum.uni-wuerzburg.de, phone: +49-931-3184111, fax: +49-931-84113.

Author contributions

A.G., E.W., D.K., S.W., B.v.E., N.W., C.R., and G.K. performed the experiments, A.G., E.A., E.W and M.E. designed experiments, M.F.R. provided critical advice and A.G., E.W. and M.E. wrote the paper.

Accession codes

ChIP-sequencing data have been deposited in the NCBI Gene Expression Omnibus under accession code GSE48602.

The authors declare no competing financial interests.

p15^{Ink4b} (*Cdkn2b)* in response to TGFbeta in tissue culture and *in vivo* [1, 2]. Miz1 also forms repressive complexes with Bcl6 and Gfi1; the Bcl6/Miz1 complex represses expression of *Cdkn1a* and *Bcl2* to control proliferation and survival of germinal center B-cells [3, 4, 5].

To test the role of Miz1 *in vivo*, we previously generated mice, in which exons that encode the POZ-domain of Miz1 are flanked by loxP sites (generating *Miz1*$^{\Delta POZ}$ mice) [6, 7]. The Miz1$^{\Delta POZ}$ protein fails to stably associate with chromatin and lacks the ability to regulate gene expression [7, 8]. Consistent with the biochemical model outlined above, some of the phenotypes observed in *Miz1*$^{\Delta POZ}$ mice can be explained by complex formation of Myc with Miz1. For example, both Myc and Miz1 are dispensable during normal skin development, but have critical functions during development of skin papillomas as repressors of *Cdkn1a* [9, 10].

In addition, Miz1 has essential functions during early B- and T-cell development that are independent of Myc [7, 11, 12]. Specifically, Miz1 is required for the expression of the T-cell receptor β-chain at the cell surface and for IL-7-dependent signal transduction [7, 12]. Since Miz1 itself is a DNA-binding protein, one model to explain these findings is that Miz1 binds and directly regulates target genes involved in signal transduction; accordingly, Myc-independent phenotypes might be due to deregulated expression of these genes. Currently, however, neither the DNA sequence to which Miz1 binds nor its direct target genes are known.

Miz1 is also highly expressed in many postmitotic cells, including neurons of the peripheral and central nervous systems (CNS) [13], arguing that Miz1 function extends beyond regulation of cell proliferation. This prompted us to use a Nestin-Cre strain to delete the POZ-domain in the CNS (*Miz1*$^{\Delta POZNes}$). We report here a genome-wide analysis of Miz1 target genes by ChIP-sequencing, gel shift analyses and microarrays that identify Miz1 as a transcriptional regulator of multiple genes involved in vesicular transport, endocytosis and autophagy.

Results

Loss of Miz1 function causes cerebellar neurodegeneration

In order to identify roles for Miz1 in neuronal cells, we crossed *Miz1*$^{flox/flox}$ mice with mice expressing Cre-recombinase under the control of the Nestin promoter [14], generating mice that express an amino-terminally truncated protein lacking the POZ-domain of Miz1 in the central nervous system (*Miz1*$^{\Delta POZNes}$) (Supplementary Figures S1a,b). Mice of the different genotypes were born at the expected Mendelian frequencies (Supplementary Figure S1c). Analysis of genomic DNA and qRT-PCR experiments confirmed that deletion of exons 3 and 4, which encode the POZ-domain, occurred efficiently in the cerebrum, cerebellum, olfactory bulb and, with a lower efficiency, in the eye, which are derived from Nestin-expressing progenitor cells (Supplementary Figure S1d,e).

Miz1$^{\Delta POZNes}$ mice initially appeared normal, but were smaller than either wild type or heterozygous littermates at five weeks after birth and this difference in size increased with age (Supplementary Figure S2a). In addition, *Miz1*$^{\Delta POZNes}$ mice progressively developed neurological symptoms characterized by slow movement, ataxia and tremor (Figure 1a). As

a result, most *Miz1*$^{\Delta POZNes}$ mice had to be sacrificed at around 18 months of age. Macroscopic analysis revealed that the overall structure of the brain was largely normal in *Miz1*$^{\Delta POZNes}$ mice except for the cerebellum. The cerebellum was of normal size in newborn animals, but its relative size decreased over time compared to wild type and heterozygous animals (Figures 1b, Supplementary Figure S2b). Within the cerebellum, both the white matter and all three layers of the grey matter (Purkinje cells, molecular layer and granular layer) were reduced in size and appeared disorganized (Supplementary Figure S2c).

Staining of calbindin, a marker for Purkinje cells, revealed disruption of the Purkinje cell layer at 10 months of age and a corresponding increase in Bergmann glia cells as documented by staining with antibodies directed against glial fibrillary acid protein (GFAP) (Figure 1c,d). The Purkinje cell layer appeared normal at four weeks of age, but was largely disrupted at 15 months of age (Supplementary Figure S2d). We also observed increased apoptosis in the granular layer (Figure 1e). This is consistent with observations that the survival of granular neurons depends on synaptic connections with Purkinje cells [15]. In order to understand why Miz1 loss has the strongest effects on Purkinje cells, we performed *in situ* hybridization and immunohistochemistry (Figure 2a,b). Both techniques revealed elevated expression of *Miz1* mRNA and protein in Purkinje cells, suggesting that these cells are particularly sensitive to the lack of a functional Miz1 protein.

Identification of Miz1 target genes and DNA binding sequence

To understand the molecular basis of this phenotype, we identified Miz1 target genes in neuronal cells. We isolated neural progenitor cells from E13.5 brain. After expansion as neurospheres in culture, we performed chromatin immunoprecipitation experiments coupled with high-throughput sequencing to systematically map Miz1 binding sites on chromatin. Statistics for all sequencing experiments are shown in Supplementary Table S1. This analysis identified 261 sites to which Miz1 bound with high occupancy (Figure 3a; see Supplementary Figure S3a for more examples and Supplementary Table S2 for a complete list). Control chromatin immunoprecipitation experiments using independent preparations of chromatin confirmed the specificity of binding (Supplementary Figure S3b). Furthermore, we used a different α-Miz1 antibody and confirmed specific binding of Miz1 to 10/10 sites identified in the genome-wide analysis relative to control regions (Supplementary Figure S3c). The majority of Miz1 binding sites were localized in core promoters close to the transcription start site, unequivocally identifying 140 Miz1-bound promoters (binding site +/− 1.5 kb of the transcription start site, Figure 3b). Comparison with ChIP-sequencing datasets from human mammary epithelial cells (MDA-MB231) showed that binding of Miz1 to these promoters is largely conserved between different cell types and species (Figure 3c; $p<5\times10^{-324}$ using a hypergeometric test).

The binding site for Miz1 on DNA is unknown. To determine whether Miz1 specifically recognizes its target promoters, we used MEME-ChIP (“Motif Analysis of Large DNA Datasets“) algorithms to search the ChIP-sequencing dataset obtained from neural progenitor cells for conserved sequence motifs in Miz1-bound chromatin. This analysis yielded an extended non-palindromic sequence that is present in the center of 181 of the 261 Miz1 bound sites (Figure 3d) ($E=4.4\times10^{-360}$; for definition of E-value, see [16]). Gel-shift

experiments using extracts of HeLa cells ectopically expressing Miz1 identified two complexes that were super-shifted with several independent Miz1 antibodies, but not with control or α-Myc antibodies; a weaker, co-migrating complex was observed in control cells (Figure 3e). Competition experiments showed that mutation of conserved nucleotides abolished binding to Miz1 to this site, whereas mutation of non-conserved nucleotides did not (Figure 3e). Virtually identical results were obtained with a recombinant Miz1 protein (Supplementary Figure S4). We concluded that this sequence constitutes a direct binding site for Miz1.

To test whether Miz1 activates transcription of it's target genes, we cloned a 1kb fragment of the *Rorc* promoter and oligonucleotides (71bps) spanning the Miz1 binding site from the *Ambra1* promoter, both covering the respective start sites of transcription, in front of a luciferase open reading frame and performed transient reporter assays. Co-expression of Miz1 stimulated expression of both constructs relative to a control vector, whereas the Miz1$^{\Delta POZ}$ protein was impaired in transactivation (Figure 4a). Similar results had been obtained previously in reporter assays using the *Cdkn2b* promoter [8, 17]. Consistent with these results, microarray analyses of RNA isolated from cerebella of wild type and Miz1$^{\Delta POZNes}$ mice showed that the expression of the 140 genes that are direct targets of Miz1 (see Figure 3c) was significantly downregulated in cerebella of *Miz1*$^{\Delta POZNes}$ mice (Figure 4b). To extend these results, we spiked a gene set enrichment analysis (GSEA) with a gene set of these Miz1-bound promoters and found that this was the most strongly downregulated and only statistically significant set of genes in this analysis (Figure 4c; p=0.000; FDR q=0.002. In this analysis, the nominal P value is calculated using an empirical phenotype-based permutation test procedure. The q value (FDR) is corrected for gene set size and multiple hypothesis testing)[18]. qRT-PCR analyses confirmed that multiple direct target genes of Miz1 were expressed at lower levels in cerebella of *Miz1*$^{\Delta POZNes}$ mice and that down-regulation of Miz1 target genes preceded the appearance of overt pathology since it was already apparent in phenotypically normal young animals (Figure 4d). In addition, expression of multiple genes specifically expressed in Purkinje cells, such as *Calbindin*, *Car8* and *Cbln1* was strongly downregulated in cerebella of 1.5 years old *Miz1*$^{\Delta POZNes}$ animals although these genes were not direct target genes of Miz1, suggesting that their expression was reduced as an indirect consequence due to the loss of Purkinje cells. Reduced expression of direct Miz1 target genes was also observed in mouse embryonic fibroblasts isolated from *Miz1*$^{\Delta POZ}$ mice, demonstrating that Miz1-dependent regulation is not restricted to the cerebellum (Supplementary Figure S5a). Ectopic expression of wild type Miz1 restored expression of Miz1 target genes (Supplementary Figure S5b). Furthermore, siRNA-mediated depletion of Miz1 decreased expression of Miz1 target genes in mouse embryo fibroblasts (Supplementary Figure S8b). Finally, immunohistochemistry as well as immunoblotting confirmed that the protein encoded by one of the Miz1 target genes, Ambra1, is expressed at lower levels in cerebella and brains of *Miz1*$^{\Delta POZNes}$ mice relative to wild type and heterozygous mice (Supplementary Figure S5c,d) and in *Miz1*$^{\Delta POZ}$ mouse embryo fibroblasts (Supplementary Figure S5e). Taken together, the data show that Miz1 activates a set of direct target genes *in vivo* and in tissue culture.

Miz1 target genes are involved in transport and autophagy

Neither Ingenuity (www.ingenuity.com), gene ontology (GO)-term, nor GSEA analysis identified statistically enriched functions or previously identified expression profiles involving Miz1 target genes that could explain the observed phenotype. Functional annotation revealed that multiple target genes of Miz1 encode proteins involved in vesicular transport pathways, endocytosis and lysosomal biogenesis (Table 1). Examples include Vps28, which is involved in sorting ubiquitinated proteins in the endosomal compartment as part of the ESCRT-I complex (Endosomal sorting complex required for transport-I) [19], Exoc2, which is part of the exocyst complex, a multi-protein complex involved in exocytosis and transport from recycling endosomes [20] as well as Pikfyve (Fab1), a phosphatidylinositol kinase that regulates vesicular transport and endocytosis [21]. Endosomal transport and lysosomal biogenesis have been implicated in late steps of autophagy; hence several target genes of Miz1 involved in vesicular transport have been linked to autophagy (Table 1 and Supplementary Table S3). In addition, several Miz1 target genes encode proteins that have been directly linked to autophagy; examples for this group include Ambra1, an activating cofactor of Beclin1, Gne and Tbc1d14 (Table 1) [22].

Since the phenotype of knock-out mice that carry brain-specific deletions of the *Atg5* or *Atg7* genes, which encode E1- and E3-like enzymes for Atg12 conjugation during autophagy, is reminiscent to that of *Miz1*$^{\Delta POZNes}$ mice, we tested whether *Miz1*$^{\Delta POZNes}$ mice display phenotypes that might indicate a defective autophagy [23, 24]. During autophagy, both monoand polyubiquitinated proteins are sequestered in specific vesicles (“autophagosomes“) that subsequently fuse with lysosomes leading to proteasome-independent degradation of long-lived proteins [25]. We therefore performed immunohistochemistry with an antibody against ubiquitin and observed a punctate staining in the body of Purkinje cells of *Miz1*$^{\Delta POZNes}$, but not control mice, arguing that ubiquitinated proteins accumulate in cytoplasmic vesicles or aggregates in these neurons (Figure 5a; for a quantification of staining see Figure 5d). In addition, strongly ubiquitin-positive cellular fragments were found in the molecular layer and the white matter of 15month-old *Miz1*$^{\Delta POZNes}$ mice, but neither in age-matched control nor in young *Miz1*$^{\Delta POZNes}$ mice, correlating with the observed phenotypes (Figure 5b,c,d). Such cellular fragments most likely corresponded to protrusions (dendrites or axons) of cerebellar neurons (Figure 5f). Biochemical fractionation showed that both poly- and monoubiquitinated proteins accumulated in an insoluble form in the cerebella of *Miz1*$^{\Delta POZNes}$ mice, but not in brains of control mice, in an age-dependent manner (Figure 5e). Importantly, proteasome activity was identical between cerebella of wild type and *Miz1*$^{\Delta POZNes}$ mice, arguing that the accumulation of ubiquitinated proteins was not due to a decrease in proteasome activity (Supplementary Figure S6a).

Defects in autophagy also cause accumulation of p62/SQSTM1 [26]. p62 acts as a receptor for ubiquitinated cargoes and delivers them to the autophagosome; p62 itself is incorporated into the autophagosome and subsequently degraded by autophagy [26]. Cerebella of *Miz1*$^{\Delta POZNes}$ mice also displayed strongly elevated levels of p62 aggregates, (Figure 5c,d). Notably, ubiquitin-positive structures in the white matter co-localize with p62; virtually identical observations have been reported for other autophagy-deficient strains of mice [27].

Furthermore, p62, like the ubiquitinated proteins, accumulated in a detergent-insoluble form (Supplementary Figure S6b). Finally, transmission electron microscopy revealed the accumulation of large polymorphic multilamellar bodies occasionally containing multivesicular or amorphous material in the Purkinje cell bodies and dendrites of *Miz1*$^{\Delta POZNes}$ mice (Figure 5f and Supplementary Figure S6c-e; for a quantitation of organelles, see Supplementary Figure S7b). These multilamellar bodies are morphologically very similar to membranous cytoplasmic bodies accumulating in autophagy-deficient neurons of Trpml1 (transient receptor potential cation channel/mucolipin1)-deficient animals, expression of which is strongly downregulated in *Miz1*$^{\Delta POZNes}$ cerebella (Table 1) [28].

Collectively, the findings suggested that Purkinje cells in *Miz1*$^{\Delta POZNes}$ mice had a defect in autophagy that could account for the phenotype of *Miz1*$^{\Delta POZNes}$ mice. Surprisingly, however, steady state levels of Lc3/Atg8 that is conjugated to phosphatidylethanolamine (Lc3-II), a marker of autophagy, were unaltered in the cerebella of *Miz1*$^{\Delta POZNes}$ mice (Supplementary Figure S7a). Furthermore, transmission electron microscopic analysis revealed strong decreases in the number of lysosomes and lipofuscin-containing vesicles, which are thought to be end-stage lysosomes, but did not detect significant changes in the number of autophagosomes (Supplementary Figure S7b). These results either indicate that autophagy is unaltered or that autophagic flux is inhibited at several steps, such that flux is low but no specific intermediates accumulate [29]. Conjugated Lc3 is degraded upon fusion of autophagosomes with lysosomes. Therefore, accumulation of Lc3 in the presence of lysosomal inhibitors can be taken as a measure of autophagic flux allowing us to distinguish between both alternatives [29].

Miz1-dependent autophagic flux

To test whether Miz1 is required for maintaining autophagic flux, we isolated primary embryonic fibroblasts from *Miz1*$^{flox/flox}$ mice expressing a Cre-ER transgene. Exposure of *Miz1*$^{flox/flox}$*Cre-ER*$^{+}$ cells to 4-OHT induced acute deletion of exons 3 and 4 and decreased expression of Miz1 target genes (Figure 6a,b). Consistent with the results obtained *in vivo*, deletion of Miz1 had little effect on Lc3 conjugation in unperturbed cells (Figure 6c). In contrast, the accumulation of conjugated Lc3 that occurs in response to inhibition of lysosomal protein degradation was significantly impaired in Miz1$^{\Delta POZ}$ cells “lys PI” lanes in Figure 6c). Addition of 4-OHT had no effect on the expression of Miz1 target genes and autophagic flux in control (*Miz1*$^{flox/flox}$) cells (Figure 6b,c), indicating that loss of functional Miz1 impairs autophagic flux. This conclusion is supported by the observation that *Miz1*$^{\Delta POZ}$ mouse embryo fibroblasts have a reduced capacity for degradation of long-lived proteins upon amino acid starvation (Supplementary Figure S8a). Notably, deletion of the POZ domain of Miz1 diminished autophagic flux both in normal medium (DMEM) and in medium depleted for amino acids (EBSS), demonstrating that Miz1 is not required for the induction of autophagy in response to amino acid starvation (Figure 6c). Consistent with this interpretation, expression of Miz1 target genes was decreased in both media (Figure 6d). Furthermore, treatment of mouse embryo fibroblasts with siRNA targeting Miz1 strongly reduced expression of multiple target genes of Miz1 involved in membrane traffic and autophagy (Supplementary Figure S8b) and diminished autophagic flux in response to

inhibition of lysosomal protein degradation (Supplementary Figure S8c). These observations confirm that the reduction of autophagic flux observed in Miz1$^{\Delta POZ}$ cells is due to loss of Miz1 function.

Consistent with the results obtained in cerebella of *Miz1*$^{\Delta POZNes}$ mice, expression of multiple target genes of Miz1 was decreased in cultured neurospheres from E13 embryos of *Miz1*$^{\Delta POZ}$ and of homozygous Miz1$^{\Delta POZNes}$ mice (Figures 6e, S8d). In contrast, effects on target gene expression were much weaker in heterozygous (*Miz*$^{flox/wt}$ *Cre*$^{+}$*)* neurospheres, correlating with the lack of phenotype of these animals (Supplementary Figure S8d). Exposure of neurospheres isolated from *Miz1*$^{flox/flox}$*Cre-ER*$^{+}$ mice to 4-OHT induced the acute deletion of exons 3 and 4 and diminished autophagic flux as documented by reduced accumulation of conjugated Lc3 in the presence of inhibitors of lysosomal protein degradation (Figure 6f,g). In contrast to the *in vivo* situation, we failed to detect accumulation of polyubiquitinated proteins in cultured neurospheres (Supplementary Figure S8e). We propose that apoptosis and subsequent cell lysis prevents the detection of poly-ubiquitinated proteins in cultured Miz1$^{\Delta POZ}$ neurospheres. Consistent with this interpretation, microarray analyses from neurospheres at different passages indicated a progressive reduction in expression of genes characteristic of neuronal progenitors Miz1$^{\Delta POZ}$ neurospheres in addition to downregulation of Miz1 target genes, suggesting that accumulation of ubiquitinated proteins might lead to the elimination of neuronal progenitors via apoptosis (Supplementary Table S4). Furthermore, transmission electron microscopy revealed the presence of multilamellar bodies in early apoptotic cells found in *Miz1*$^{\Delta POZ}$ neurospheres (Supplementary Figure S8f).

The findings suggested that the lack of changes in steady state levels of Lc3 conjugation is observed due to blockade of autophagic flux at several steps. Of the Miz1 target genes, *Ambra1* is required for autophagosome formation and Lc3-conjugation in mammalian cells [30]. Several members of the ESCRT complex have been implicated in mammalian autophagy, but none of the Miz1 target genes listed in Supplementary Table S2. We therefore used siRNA to deplete Vps28 in neuroblastoma cells that stably expressed Lc3-GFP and Lamp1-RFP, which marks lysosomes. Upon depletion of Vps28, Lc3 accumulated in vesicles (Figure 6h). Importantly, Lc3 staining did not overlap with staining for the lysosomal marker Lamp1, indicative of a late block in autophagy (Figure 6h). These findings are consistent with observations in Drosophila cells [31]. We concluded that target genes of Miz1 are required at early and late steps of autophagy.

Discussion

We showed here that Miz1 has a critical function in maintaining the viability of Purkinje cells in the cerebellum *in vivo*. In the absence of functional Miz1, cerebella undergo progressive neurodegeneration, which is characterized by an age-dependent accumulation of ubiquitinated proteins and of p62, indicative of defective autophagy.

In order to explain these phenotypes, we used ChIP-sequencing to show that Miz1 binds to approximately 260 target sites in neuronal progenitor cells. Target sites of Miz1 had an extended non-palindromic consensus sequence as might be expected for a protein with

multiple (13) zinc fingers. Biochemical analysis confirmed that Miz1 directly bound to this sequence. Comparison with data obtained in human mammary epithelial cells (MDA-MB231) showed that these direct target genes were largely conserved between different tissues and species. Miz1 binding sites were predominantly found in core promoters, close to the transcription start site. Reporter assays and comparison with gene expression data showed that Miz1 activates transcription upon binding to its cognate DNA sequence, arguing that the phenotype of *Miz1*$^{\Delta POZNes}$ mice was due to reduced expression of Miz1 target genes. Comparison with published microarray data showed that the direct Miz1 target genes described here are not subject to regulation by Myc, arguing that their expression may reflect Myc-independent functions of Miz1 (Supplementary Table S5).

Defects in distinct cellular processes can lead to accumulation of polyubiquitinated proteins [32, 33]. One is autophagy and one of the Miz1 target genes described here, *Ambra1*, is a bona-fide autophagy gene [30]; other target genes encode regulators of autophagy (e.g. Tbc1d14 and Pdcd5) (see Supplementary Table S3 for references). Late steps of autophagy involve the fusion of autophagosomes with endosomal vesicles and ultimately lysosomes [22, 34]. As a result, defects in the progression of endosomes along the endosomal-lysosomal pathway, such as dysfunction of ESCRT complex proteins, indirectly cause defects in autophagy and accumulation of polyubiquitinated proteins [35]. Multiple proteins encoded by target genes of Miz1 (e.g. Vps28, Pikfyve/Fab1, Rorc) were involved in vesicular transport, late steps of autophagosome processing and in fusion of endosomes with lysosomes. We confirmed that depletion of mammalian Vps28, a direct target gene of Miz1, caused a late block in autophagy. We propose that autophagic flux is reduced in *Miz1*$^{\Delta POZ}$ cells due to the decreased expression of proteins that act at both early and late stages of the autophagic pathway. This model can explain why steady-state levels of Lc3 conjugation were unaffected by loss of Miz1 *in vivo* and in cell culture [29]. In post-mitotic cells, autophagy is critical for removal of damaged organelles and toxic protein aggregates; notably, deletion of *Atg5* or *Atg7* in the CNS has the strongest effect on Purkinje cells, similar to what is observed in Miz1$^{\Delta POZNes}$ mice, arguing that survival of these cells is particularly dependent on autophagy [23, 24, 36, 37]. The reduction of autophagic flux observed in *Miz1*$^{\Delta POZNes}$ mice could therefore account for their progressive neurodegeneration. Notably, the neurodegenerative phenotype of Miz1$^{\Delta POZNes}$ mice is weaker than that of *Atg5* or *Atg7* knockout mice, most likely due to residual autophagic flux in Miz1$^{\Delta POZNes}$ cells and, by inference, in cerebella of Miz1$^{\Delta POZNes}$ mice. Since several target genes of Miz1 encode proteins that are required for intracellular trafficking of multiple cell surface receptors and since regulated transport to the cell surface and endocytosis are critical for the function of the TCR and IL-7 receptors that are functionally deficient in Miz1$^{\Delta POZ}$ lymphocytes, we propose that the target genes identified here can also account for other phenotypes observed in Miz1$^{\Delta POZ}$ animals [38, 39, 40, 41, 42]. Several other transcription factors, such as p53, TFEB and the FoxO family of factors have been implicated in the transcriptional control of autophagy [43, 44, 45] . Notably, there is little overlap in the direct target genes of these factors with those bound by Miz1, suggesting that the precise process within the overall autophagic process that is enhanced by each factor may differ functionally and reflect the specific stimulus or stress response that activates each factor.

Previous work had shown that the ribosomal assembly factor, nucleophosmin, is a co-activator of Miz1 [46]. In growing cells, nucleophosmin is retained in the nucleolus by the ribosomal protein, Rpl23. Nucleophosmin is released into the nucleolus when Rpl23 levels fall, linking transactivation by Miz1 to defects in ribosome biogenesis. Together with the findings reported here, the data argue that Miz1 is a stress-responsive factor that balances biosynthetic capacity and cell growth with nutrient and energy supply in addition to promoting cell cycle arrest.

Methods

Mice

Miz1$^{flox/flox}$ and *Miz1*$^{+/\Delta POZ}$ mice were crossed to each other and to Nestin-Cre mice [14] to obtain *Miz1*$^{\Delta POZNes}$ mice. Mice were genotyped by standard PCRs using three different primers listed in Supplementary Table S4 (genomic PCRs). Mice of both sexes between 0 and 18 months (as indicated in figure legends) were used and all mice were included in the analysis. Unless indicated otherwise, mice that carry one or two wild type alleles of *Miz1* and *Miz1*^{flox} mice that do not express Nestin-Cre were collectively used as control mice. Speed of movement was measured by placing mice on a grid and determining distance covered per time. To measure motor coordination, mice were trained for three days to the rotarod (Ugo Basile). Subsequently, the time each animal was able to run at a constant speed of 21 rpm was determined. The circumference of the cerebellum was measured and used to estimate surface area. All experiments were carried out according to German law and are approved by an institutional panel (Tierschutzkommission der Regierung von Unterfranken).

Immunofluorescence, immunohistochemistry and histology

All staining were performed on tissue sections collected from OCT- or paraffin-embedded tissues. The following primary antibodies were used: α-Calbindin (1:100, Sigma, C9848), α-glial acidic fibrillary protein (GFAP) (OPA1-06100, Pierce), α-Miz1 (1:100, H190, Santa Cruz), α-Ubiquitin (1:100, MBL, MK 11-3), α-p62 (1:1000, MBL, pm045). Detection of primary antibodies was carried out with appropriate peroxidase- or fluorochrome-coupled secondary antibodies. Sections were counterstained with hematoxylin. TUNEL staining was performed using an *in situ* cell death detection kit (Roche). Klüver-Barrera and H&E staining was performed according to standard procedures. Pictures were taken with a Leica DM 6000B microscope.

Cell culture

To isolate neuronal progenitor cells (NPCs), forebrains of E13.5 *Miz1*$^{+/+}$, *Miz1*$^{\Delta POZ}$ or *Miz1*$^{flox/flox}$*Cre-ER*$^{+}$ embryos were cut in small pieces, digested with trypsin and filtered through sterile gauze. Cells were cultivated in 2:1 DMEM/F12 supplemented with 1×B27 (Life technologies), 20 ng/μl EGF (Biomol), 20 ng/μl basic FGF (Biomol), 1 μg/ml fungizone (Gibco) and Penicillin/Streptomycin (PAA). NPCs were passaged every seven days. Mouse embryo fibroblasts (MEFs) were isolated from E13.5 *Miz1*$^{flox/flox}$*Cre-ER*$^{+}$ and *Miz1*$^{flox/flox}$*Cre-ER*$^{-}$ embryos. To induce recombination in *Miz1*$^{flox/flox}$*Cre-ER*$^{+}$ NPCs or MEFs, cells were incubated with 200 nM 4-OHT for 3-4 days. Cells were passaged and treated with 20 μM Leupeptin and 20 mM NH_4Cl for 30 minutes (NPCs) or 2 hours (MEFs)

in NPC medium or DMEM and EBSS (Earle's balanced salt solution) (MEFs). To measure degradation of long-lived proteins, cells were labelled with 5 μCi of ^{35}S-Met/Cys (Hartmann) for 3 h, washed and incubated for 17 h to release short-lived proteins. To block autophagy, cells were incubated with 10 mM 3-methyl-adenine (Tocris Bioscince) for 3 h. After washing, cells were incubated with EBSS or DMEM in the presence/absence of 3-methyl-adenine for 4 h. TCA-cleared supernatant and TCA-washed cells were measured with a scintillation counter. Long-lived protein degradation was calculated by dividing the released radioactivity by total radioactivity.

Chromatin immunoprecipitation and parallel sequencing

For chromatin immunoprecipitation (ChIP), cells were cross-linked with 1 % formaldehyde at 37°C for 10 min. Sonication was carried out after swelling in a Bransson sonifier until the majority of fragments showed nucleosomal size. α-Miz1 antibodies (neuronal progenitors: H190; MDA cells: G18 (Santa Cruz)) were coupled to ProteinA/G-Dynabeads (Invitrogen) and used for immunoprecipitation. DNA was purified with Qiagen PCR purification kit after elution of the bound chromatin with 1% SDS and reversion of the crosslink. ChIP DNA was end repaired and A-tailed. Illumina adaptors were ligated to the ChIP DNA fragments. 175 -225bp size fractions were cut out from a 1% agarose gel, extracted by Qiagen gel extraction kit and enriched by 18 cycles of PCR amplification. Library size was controlled with the Experion-system (BioRad) and subsequently quantified by picogreen assay and sequenced on an Illumina GAIIx sequencer. Only reads passing the internal Illumina raw data-filter were considered. Resulting fastq files were used for alignment to a precompiled reference index (neuronal progenitor cells: mm9, MDA: hg19) with BOWTIE [47]. Peaks were called by MACS [48] using data from the input sample as control and determining a p-value of 10^{10}. GEO accession number for the ChIP-sequencing results is: GSE48602.

To compare the Miz1 peaks in neuronal progenitor and MDA-MB231 cells, a hypergeometric distribution was used: first the total number of base pairs covered by peaks in each dataset was calculated (NPC 41,500bp and MDA-MD231 4,47494bp), and second the number of overlapping base pairs of MDA-MD231 and NPCs peaks was counted (33,176bp). As population size all murine promoter regions (+/−1.5kb around a TSS; total 93,582,000bp) were used.

Gene Expression

Total cellular RNA was isolated from whole cerebella or from neurospheres using RNAeasy (Qiagen) including on-column DNA digestion (microarray-analysis) or extraction with peqGOLD (Peqlab) for qRT-PCR. For isolation of RNA from cerebellum, tissue samples were placed into peqGOLD and homogenized with an ultra-turrax. For microarray analyses, RNA was additionally treated with DNAase on an RNAeasy column. Agilent Mouse Genome Microarray 4×44 K v2 was used for the analysis of the gene expression. For qRT-PCR, the first-strand was synthesized with M-MLV Reverse Transcriptase (Invitrogen) and random hexamer primers (Roche). Primer sequences are shown in Supplementary Table S6. For *in situ* hybridizations, DNA corresponding to exons 3 and 4 of murine *Miz1* was cloned into pBluescript KS+ vector and used for synthesis of sense and antisense probe.

ArrayExpress accession numbers for the microarray results are: E-MEXP-3878 (cerebella) and E-MEXP-3883 (neurospheres).

Cell fractionation and immunoblotting

Detergent-soluble and -insoluble protein fractions from mouse brains were prepared as described [23]. Briefly, after homogenization, cells were lysed with 0.5 % Triton X-100. After centrifugation the pellet was re-suspended in 1 % SDS. After SDS-PAGE proteins were transferred on PVDF-membrane and immunostained for ubiquitinated proteins (07-375, upstate; MK-11-3, MBL). For immunoblotting of Lc3 in MEFs and NPCs, cells were lysed in buffer containing 50 mM Hepes-KOH, pH 7.5, 150 mM NaCl, 100 mM NaF, 10 mM EDTA, 10 mM $Na_4P_2O_7$. Immunoblots were probed with antibodies directed against Lc3 (1:1000, MBL, PM036), α-vinculin (1:10.000, Sigma) and α-tubulin (1:1000, Chemicon).

Electrophoretic mobility shift assay (EMSA)

GST-Miz1$^{\Delta POZ}$ protein was expressed in *E. coli* (BL-21) and affinity purified using a glutathione-sepharose (GE Healthcare) column. After elution with glutathione, purity was controlled with a Coomassie Brilliant Blue-stained SDS-PAGE. Dignam nuclear extracts were prepared from HeLa cells transiently transfected with pCDNA3-Miz1. For labeling, 25 pmol of annealed oligonucleotides were labeled using 0.15 mCi γ^{32}P-ATP (Hartmann) and 25U of PNK (NEB) and purified on a G50 column (GE). 1 µl of purified probe was incubated with 2 µl of nuclear extract (~ 2 mg/ml) in the presence of 20 mM Hepes-KOH , pH 7.9, 10 % (v/v) glycerol, 105 mM NaCl, 2 mM $MgCl_2$, 50 µM EDTA, 0.25 µg/µl salmon sperm DNA, 1.5 mM DTT, and protease- and phosphatase-inhibitors (Sigma) in a 20 µl reaction. For supershifts 1 µg of antibody was added (Miz1: H190, G18, C19 (all Santa Cruz) Control: rabbit/mouse IgG). After 10min incubation at room temperature, samples were separated on a 5 % PAA-/0.5× TBE-gel for 5h at 180V and exposed on phosphoimager storage screens.

Transmission electron microscopy

Female mice of different genotypes (3 *Miz1*$^{\Delta POZNes}$ mice and 3 control mice, 11-15 months of age) were perfusion-fixed in deep anesthesia via the left ventricle using, after a brief pre-rinse with heparinized saline, 4 % PFA and 2.5% glutaraldehyde (GA) in 0.1 M cacodylate buffer pH 7.3 - 7.4 (CB). After dissection of the brain and postfixation for at least 18 hours, small blocks of cerebellar tissue were taken from a cerebellar hemisphere of each mouse, washed in CB, osmicated in 2% osmium tetroxide in CB for 2 hours, dehydrated in acetone and embedded in Spurr's medium. Contralateral hemispheres were washed in PBS, cut into coronal 150 µm vibratome sections, osmicated in 1 % osmium tetroxide in PBS for 1 hour, dehydrated in ethanol and flat-embedded in Epon Ultrathin sections were contrasted with uranyl acetate and lead citrate and observed in a Leo 912 AB electron microscope (Zeiss NTS, Oberkochen, Germany). Both embedding methods yielded equivalent ultrastructural details for *Miz1*$^{\Delta POZNes}$ specimens.

In situ Hybridization (ISH)

Dissected brains were frozen in 2-methylbutane and stored at −80°C. Serial cryosections (15 μm) were thaw-mounted on microscopic slides, fixed in 4% paraformaldehyde in PBS and stored in 100% ethanol at 4°C. ISH was carried out using chromogenic detection.

Transient transfection assays

PCR fragments of the human *Ambra1* and *Rorc* promotor were cloned in a pGL4 plasmid (Clontech). HEK293 cells were transiently transfected (PEI) with the reporter constructs, Miz-WT and Miz$^{\Delta POZ}$ expression plasmids and CMV-βgal plasmid. Cells were harvested after 48 h, luciferase and β-galactosidase activity was measured according to the manufacture's protocol. Endogenous Vps28 protein was depleted in SHEP neuroblastoma cells stably expressing Lc3-GFP [49] and Lamp1-RFP [50] by siRNA (Dharmacon).

Long-lived protein degradation assays

Degradation of long lived proteins was measured according to [51]. Cells were labeled with 5 μCi of ^{35}S-Met/Cys (Hartmann) for 3 h, washed and incubated for 17 h to release short-lived proteins. To block autophagy, cells were partially incubated with 10 mM 3-methyl-adenine (Tocris Bioscience) for 3 h. After another washing, cells were incubated with EBSS or DMEM in the presence/absence of 3-methyl-adenine for 4 h. TCA-cleared supernatant and TCA-washed cells were measured with a scintillation counter. Long-lived protein degradation was calculated by dividing the released radioactivity by total radioactivity.

Determination of proteasomal activity

Proteasomal activity in cerebella of ΔPOZ and control mice was measured with a Proteasome Activity Assay Kit (Abcam). Fluorescence was measured with a microtiter plate reader (Tecan) in the presence/absence of MG132 after 15 min at 37°C for 100 min. The MG132-sensitive increase of fluorescence at 350/440 nm was considered as proteasomal activity.

Supplementary Material

Refer to Web version on PubMed Central for supplementary material.

Acknowledgments

We thank Michael Krause, Florian Finkernagel and Lukas Rycek for performing and analyzing the microarray analyses, Angela Grün, Renate Metz and Barbara Bauer for excellent technical assistance and members of the Eilers laboratory for comments on the manuscript. This work was supported the Deutsche Forschungsgemeinschaft via SFB 581 (M.E. and E.A.) and via grant 222/5-3 (to M.E.), by the NCI CA-096832 and CA-21765 (MFR), The Anderson Fellowship (DK), and the American Lebanese Syrian Charities of St Jude Children's Research Hospital.

References

1. Gebhardt A, Frye M, Herold S, Benitah SA, Braun K, Samans B, et al. Myc regulates keratinocyte adhesion and differentiation via complex formation with Miz1. J Cell Biol. 2006; 172(1):139–149. [PubMed: 16391002]

2. van Riggelen J, Muller J, Otto T, Beuger V, Yetil A, Choi PS, et al. The interaction between Myc and Miz1 is required to antagonize TGFbeta-dependent autocrine signaling during lymphoma formation and maintenance. Genes & development. 2010; 24(12):1281–1294. [PubMed: 20551174]
3. Phan RT, Saito M, Basso K, Niu H, Dalla-Favera R. BCL6 interacts with the transcription factor Miz-1 to suppress the cyclin-dependent kinase inhibitor p21 and cell cycle arrest in germinal center B cells. Nat Immunol. 2005; 6(10):1054–1060. [PubMed: 16142238]
4. Saito M, Novak U, Piovan E, Basso K, Sumazin P, Schneider C, et al. BCL6 suppression of BCL2 via Miz1 and its disruption in diffuse large B cell lymphoma. Proceedings of the National Academy of Sciences of the United States of America. 2009; 106(27):11294–11299. [PubMed: 19549844]
5. Basu S, Liu Q, Qiu Y, Dong F. Gfi-1 represses CDKN2B encoding p15INK4B through interaction with Miz-1. Proceedings of the National Academy of Sciences of the United States of America. 2009; 106(5):1433–1438. [PubMed: 19164764]
6. Gebhardt, A.; Kosan, C.; Herkert, B.; Moroy, T.; Lutz, W.; Eilers, M., et al. Journal of cell science. Vol. 120. Pt 15: 2007. Miz1 is required for hair follicle structure and hair morphogenesis.; p. 2586-2593.
7. Kosan C, Saba I, Godmann M, Herold S, Herkert B, Eilers M, et al. Transcription factor miz-1 is required to regulate interleukin-7 receptor signaling at early commitment stages of B cell differentiation. Immunity. 2010; 33(6):917–928. [PubMed: 21167753]
8. Herold S, Wanzel M, Beuger V, Frohme C, Beul D, Hillukkala T, et al. Negative regulation of the mammalian UV response by Myc through association with Miz-1. Mol Cell. 2002; 10(3):509–521. [PubMed: 12408820]
9. Oskarsson T, Essers MA, Dubois N, Offner S, Dubey C, Roger C, et al. Skin epidermis lacking the c-Myc gene is resistant to Ras-driven tumorigenesis but can reacquire sensitivity upon additional loss of the p21Cip1 gene. Genes & development. 2006; 20(15):2024–2029. [PubMed: 16882980]
10. Honnemann J, Sanz-Moreno A, Wolf E, Eilers M, Elsasser HP. Miz1 is a critical repressor of cdkn1a during skin tumorigenesis. PLoS One. 2012; 7(4):e34885. [PubMed: 22509363]
11. Saba I, Kosan C, Vassen L, Moroy T. IL-7R-dependent survival and differentiation of early T-lineage progenitors is regulated by the BTB/POZ domain transcription factor Miz-1. Blood. 2011; 117(12):3370–3381. [PubMed: 21258009]
12. Saba I, Kosan C, Vassen L, Klein-Hitpass L, Moroy T. Miz-1 is required to coordinate the expression of TCRbeta and p53 effector genes at the pre-TCR “beta-selection” checkpoint. J Immunol. 2011; 187(6):2982–2992. [PubMed: 21841135]
13. Lein ES, Hawrylycz MJ, Ao N, Ayres M, Bensinger A, Bernard A, et al. Genome-wide atlas of gene expression in the adult mouse brain. Nature. 2007; 445(7124):168–176. [PubMed: 17151600]
14. Tronche F, Kellendonk C, Kretz O, Gass P, Anlag K, Orban PC, et al. Disruption of the glucocorticoid receptor gene in the nervous system results in reduced anxiety. Nature genetics. 1999; 23(1):99–103. [PubMed: 10471508]
15. Lossi L, Mioletti S, Merighi A. Synapse-independent and synapse-dependent apoptosis of cerebellar granule cells in postnatal rabbits occur at two subsequent but partly overlapping developmental stages. Neuroscience. 2002; 112(3):509–523. [PubMed: 12074894]
16. Machanick P, Bailey TL. MEME-ChIP: motif analysis of large DNA datasets. Bioinformatics. 2011; 27(12):1696–1697. [PubMed: 21486936]
17. Staller P, Peukert K, Kiermaier A, Seoane J, Lukas J, Karsunky H, et al. Repression of p15INK4b expression by Myc through association with Miz-1. Nature cell biology. 2001; 3(4):392–399.
18. Subramanian A, Tamayo P, Mootha VK, Mukherjee S, Ebert BL, Gillette MA, et al. Gene set enrichment analysis: a knowledge-based approach for interpreting genome-wide expression profiles. Proceedings of the National Academy of Sciences of the United States of America. 2005; 102(43):15545–15550. [PubMed: 16199517]
19. Katzmann DJ, Babst M, Emr SD. Ubiquitin-dependent sorting into the multivesicular body pathway requires the function of a conserved endosomal protein sorting complex, ESCRT-I. Cell. 2001; 106(2):145–155. [PubMed: 11511343]
20. Langevin J, Morgan MJ, Sibarita JB, Aresta S, Murthy M, Schwarz T, et al. Drosophila exocyst components Sec5, Sec6, and Sec15 regulate DE-Cadherin trafficking from recycling endosomes to the plasma membrane. Dev Cell. 2005; 9(3):365–376. [PubMed: 16224820]

21. Ikonomov OC, Sbrissa D, Foti M, Carpentier JL, Shisheva A. PIKfyve controls fluid phase endocytosis but not recycling/degradation of endocytosed receptors or sorting of procathepsin D by regulating multivesicular body morphogenesis. Mol Biol Cell. 2003; 14(11):4581–4591. [PubMed: 14551253]
22. Rubinsztein DC, Shpilka T, Elazar Z. Mechanisms of autophagosome biogenesis. Curr Biol. 2012; 22(1):R29–34. [PubMed: 22240478]
23. Hara T, Nakamura K, Matsui M, Yamamoto A, Nakahara Y, Suzuki-Migishima R, et al. Suppression of basal autophagy in neural cells causes neurodegenerative disease in mice. Nature. 2006; 441(7095):885–889. [PubMed: 16625204]
24. Komatsu M, Waguri S, Chiba T, Murata S, Iwata J, Tanida I, et al. Loss of autophagy in the central nervous system causes neurodegeneration in mice. Nature. 2006; 441(7095):880–884. [PubMed: 16625205]
25. Kirkin V, McEwan DG, Novak I, Dikic I. A role for ubiquitin in selective autophagy. Mol Cell. 2009; 34(3):259–269. [PubMed: 19450525]
26. Komatsu M, Waguri S, Koike M, Sou YS, Ueno T, Hara T, et al. Homeostatic levels of p62 control cytoplasmic inclusion body formation in autophagy-deficient mice. Cell. 2007; 131(6):1149–1163. [PubMed: 18083104]
27. Liang CC, Wang C, Peng X, Gan B, Guan JL. Neural-specific deletion of FIP200 leads to cerebellar degeneration caused by increased neuronal death and axon degeneration. The Journal of biological chemistry. 2010; 285(5):3499–3509. [PubMed: 19940130]
28. Curcio-Morelli C, Charles FA, Micsenyi MC, Cao Y, Venugopal B, Browning MF, et al. Macroautophagy is defective in mucolipin-1-deficient mouse neurons. Neurobiology of disease. 2010; 40(2):370–377. [PubMed: 20600908]
29. Mizushima N, Yoshimori T, Levine B. Methods in mammalian autophagy research. Cell. 2010; 140(3):313–326. [PubMed: 20144757]
30. Fimia GM, Stoykova A, Romagnoli A, Giunta L, Di Bartolomeo S, Nardacci R, et al. Ambra1 regulates autophagy and development of the nervous system. Nature. 2007; 447(7148):1121–1125. [PubMed: 17589504]
31. Rusten TE, Vaccari T, Lindmo K, Rodahl LM, Nezis IP, Sem-Jacobsen C, et al. ESCRTs and Fab1 regulate distinct steps of autophagy. Curr Biol. 200717(20):1817–1825. [PubMed: 17935992]
32. Jaeger PA, Wyss-Coray T. All-you-can-eat: autophagy in neurodegeneration and neuroprotection. Molecular neurodegeneration. 2009; 4:16. [PubMed: 19348680]
33. Kroemer G, White E. Autophagy for the avoidance of degenerative, inflammatory, infectious, and neoplastic disease. Curr Opin Cell Biol. 2010; 22(2):121–123. [PubMed: 20202808]
34. Eskelinen EL. Maturation of autophagic vacuoles in Mammalian cells. Autophagy. 2005; 1(1):1–10. [PubMed: 16874026]
35. Lee JA, Beigneux A, Ahmad ST, Young SG, Gao FB. ESCRT-III dysfunction causes autophagosome accumulation and neurodegeneration. Curr Biol. 2007; 17(18):1561–1567. [PubMed: 17683935]
36. Levine B, Kroemer G. Autophagy in the pathogenesis of disease. Cell. 2008; 132(1):27–42. [PubMed: 18191218]
37. Madeo F, Eisenberg T, Kroemer G. Autophagy for the avoidance of neurodegeneration. Genes & development. 2009; 23(19):2253–2259. [PubMed: 19797764]
38. Rusten TE, Rodahl LM, Pattni K, Englund C, Samakovlis C, Dove S, et al. Fab1 phosphatidylinositol 3-phosphate 5-kinase controls trafficking but not silencing of endocytosed receptors. Mol Biol Cell. 2006; 17(9):3989–4001. [PubMed: 16837550]
39. Vaccari T, Rusten TE, Menut L, Nezis IP, Brech A, Stenmark H, et al. Comparative analysis of ESCRT-I, ESCRT-II and ESCRT-III function in Drosophila by efficient isolation of ESCRT mutants. Journal of cell science. 2009; 122(Pt 14):2413–2423. [PubMed: 19571114]
40. Guertin DA, Stevens DM, Thoreen CC, Burds AA, Kalaany NY, Moffat J, et al. Ablation in mice of the mTORC components raptor, rictor, or mLST8 reveals that mTORC2 is required for signaling to Akt-FOXO and PKCalpha, but not S6K1. Dev Cell. 2006; 11(6):859–871. [PubMed: 17141160]

41. McLeod IX, Zhou X, Li QJ, Wang F, He YW. The class III kinase Vps34 promotes T lymphocyte survival through regulating IL-7Ralpha surface expression. J Immunol. 2011; 187(10):5051–5061. [PubMed: 22021616]

42. Geisler C. TCR trafficking in resting and stimulated T cells. Critical reviews in immunology. 2004; 24(1):67–86. [PubMed: 14995914]

43. Crighton D, Wilkinson S, O'Prey J, Syed N, Smith P, Harrison PR, et al. DRAM, a p53-induced modulator of autophagy, is critical for apoptosis. Cell. 2006; 126(1):121–134. [PubMed: 16839881]

44. Settembre C, Di Malta C, Polito VA, Garcia Arencibia M, Vetrini F, Erdin S, et al. TFEB links autophagy to lysosomal biogenesis. Science. 2011; 332(6036):1429–1433. [PubMed: 21617040]

45. Zhao J, Brault JJ, Schild A, Cao P, Sandri M, Schiaffino S, et al. FoxO3 coordinately activates protein degradation by the autophagic/lysosomal and proteasomal pathways in atrophying muscle cells. Cell metabolism. 2007; 6(6):472–483. [PubMed: 18054316]

46. Wanzel M, Russ AC, Kleine-Kohlbrecher D, Colombo E, Pelicci PG, Eilers M. A ribosomal protein L23-nucleophosmin circuit coordinates Mizl function with cell growth. Nature cell biology. 2008; 10(9):1051–1061.

47. Langmead B. Aligning short sequencing reads with Bowtie. Curr Protoc Bioinformatics. 2010 Chapter 11: Unit 11.17.

48. Feng J, Liu T, Qin B, Zhang Y, Liu XS. Identifying ChIP-seq enrichment using MACS. Nat Protoc. 2012; 7(9):1728–1740. [PubMed: 22936215]

49. Fung C, Lock R, Gao S, Salas E, Debnath J. Induction of autophagy during extracellular matrix detachment promotes cell survival. Mol Biol Cell. 2008; 19(3):797–806. [PubMed: 18094039]

50. Zoncu R, Sabatini DM. Cell biology. The TASCC of secretion. Science. 2011; 332(6032):923–925. [PubMed: 21596981]

51. Bauvy C, Meijer AJ, Codogno P. Assaying of autophagic protein degradation. Methods Enzymol. 2009; 452:47–61. [PubMed: 19200875]

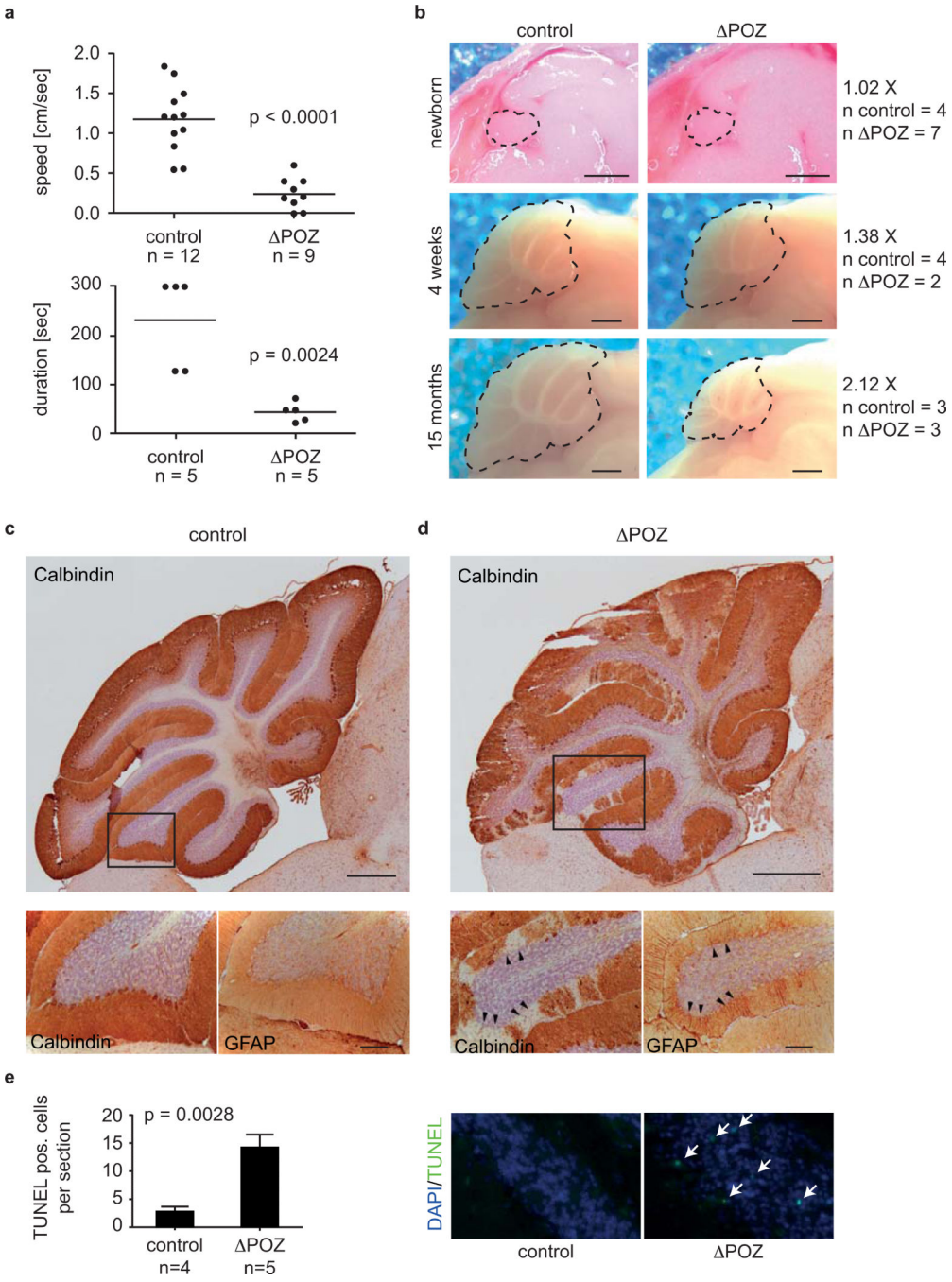

Figure 1. Phenotype of *Miz1*$^{\Delta POZNes}$ mice

(a) *Miz1*$^{\Delta POZNes}$ mice move slowly and lack motor co-ordination. The panel shows the average speed of movement and time on a rotarod (maximum: 300 sec) maintained at constant speed of control and age-matched *Miz1*$^{\Delta POZNes}$ mice. The average age of mice tested was 16 months. p-values were calculated using an unpaired two-tailed Student's t-test (The number of animals tested is shown below each graph).

(b) Defect of cerebellar growth in *Miz1*$^{\Delta POZNes}$ mice. The panels show sagittal sections of brains of control and *Miz1*$^{\Delta POZNes}$ mice at the indicated age. Dotted lines show the

circumference of the cerebellum. For each mouse, the cerebellar surface area was determined; numbers show the ratio between control and *Miz1*$^{\Delta POZNes}$ mice. The number of mice analyzed for each genotype is indicated on the right. Scale bar: 1mm.

(c,d): Histology of the cerebellum. Sections of the cerebellum of 11 month-old control (c) and *Miz1*$^{\Delta POZNes}$ (d, please note different scale) mice were stained with antibodies directed against calbindin, a marker for Purkinje cells, and GFAP, a marker for Bergman glial cells. Boxes indicate the area of a detail picture in the overviews. GFAP staining is shown for adjacent section (arrowheads: regions of missing Purkinje cells). Scale bar: Upper panels: 500 μm, lower panels: 100 μm.

(e) Enhanced apoptosis in the granular layer of cerebella in *Miz1*$^{\Delta POZNes}$ mice. The upper panel shows representative TUNEL staining of cerebella of age-matched control and *Miz1*$^{\Delta POZNes}$ mice. The lower panel shows a quantification of staining observed in four control and five *Miz1*$^{\Delta POZNes}$ mice. Error bars show standard error of the mean (SEM). p-value was calculated using an unpaired two-tailed Student's t-test.

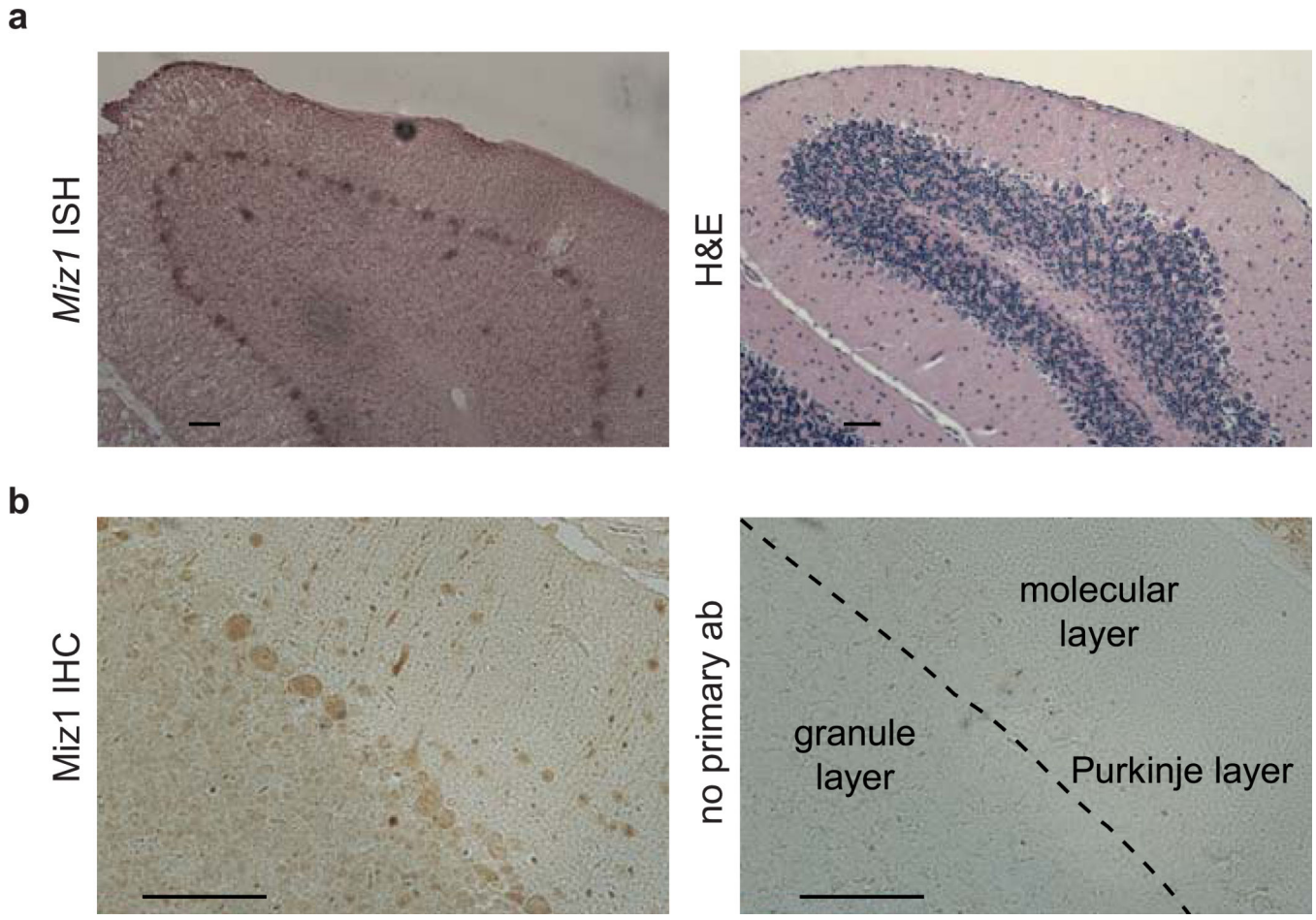

Figure 2. Miz1 is highly expressed in Purkinje cells

(a) *In-situ* hybridization (ISH) documenting expression of *Miz1* mRNA in Purkinje cells of the cerebellum in wild type mice. Left panel shows *in situ* hybridization, right panel shows H&E staining. Scale bar: 50 μm.

(b) Immunohistochemistry (IHC) documenting the presence of Miz1 in the nuclei of Purkinje cells. The panel on the left shows staining with $\tilde{\alpha}MiZ1$ (H190) antibody, staining on the right is a control staining lacking primary antibody. Scale bar: 50 μm.

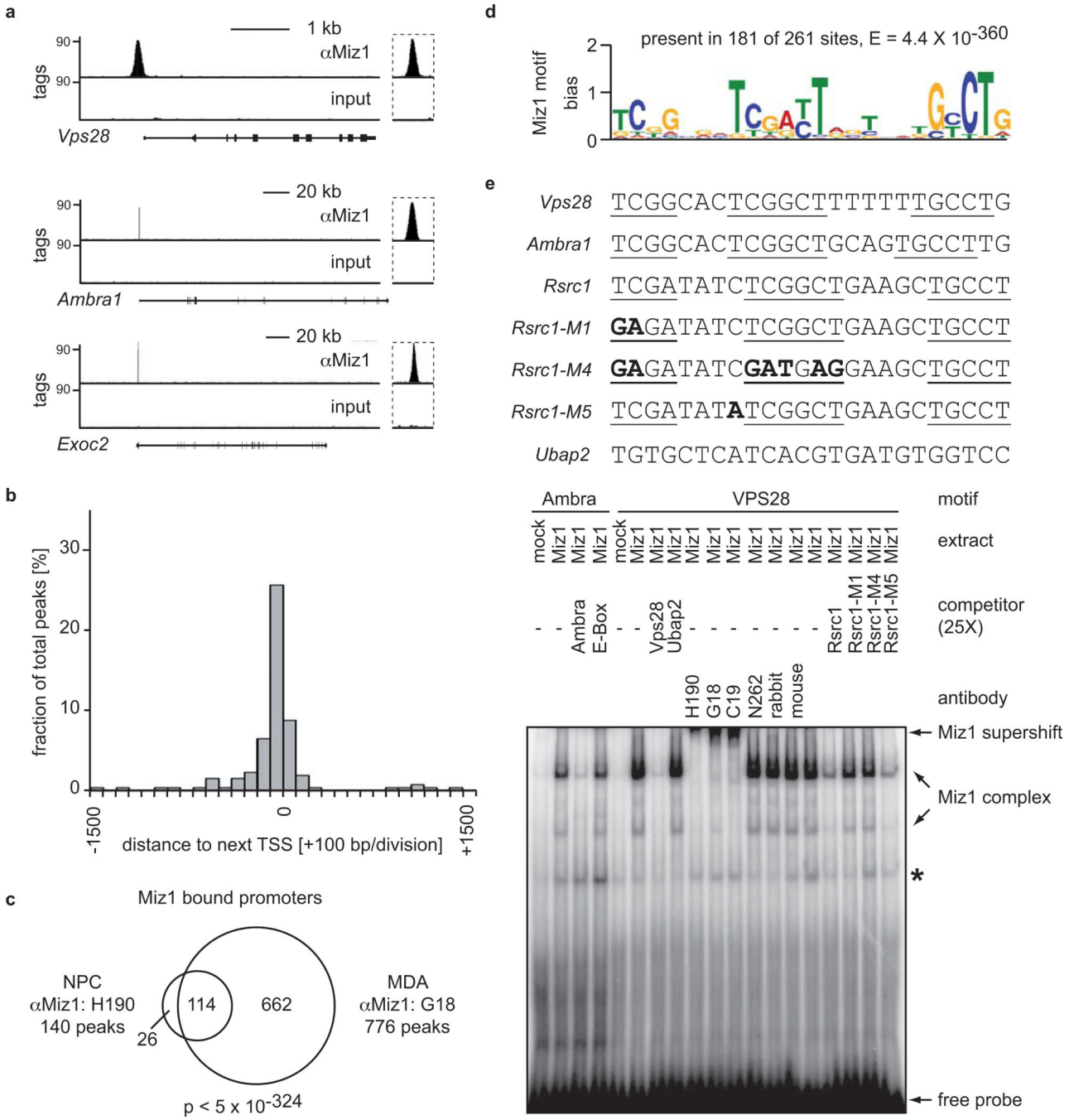

Figure 3. Identification of Miz1 target genes and DNA binding sequence

(a) Representative examples for ChIP-sequencing traces obtained from neuronal progenitor cells using an α-Miz1 antibody. Input traces are shown as negative control. For each gene, the intron/exon structure is shown below the traces with exons indicated as vertical bars and the transcriptional start site at the left. An enlarged picture of the peak region is shown on the right.

(b) Miz1 binds predominantly to core promoters. The panel shows a histogram of the percentage of promoters with the indicated distances between the peak of the Miz1 binding

site and the next transcriptional start site (TSS). 140/261 (54 %) of all peaks are located in core promoters (+/− 1.5 kb).

(c) Miz1 binding is conserved across different cell types and species. The plot shows a Venn diagram documenting the overlap in Miz1-bound promoters between murine neuronal progenitor cells (NPCs) and human MDA-MB231 cells (a mammary epithelial tumor cell line). The p-value was calculated using a hypergeometric test. Note that different α-Miz1 antibodies (H190, G18) were used for the analysis of mouse and human Miz1 binding sites.

(d) Miz1 binding sites contain a conserved sequence element. Sequences (+/−50bp) around all 261 Miz1 binding sites observed in NPCs were analyzed by MEME-ChIP [16].

(e) Electrophoretic-shift mobility assay documenting binding of Miz1 to the conserved sequence element (“Miz1-binding motif”). Nuclear extracts from control HeLa cells (“mock”) or cells ectopically expressing Miz1 were incubated with radioactive oligonucleotides spanning the Miz1 binding motif of the *Ambra1*- and *Vps28*-promoters. Where indicated, binding reactions included a 25-fold excess of non-labeled oligonucleotides (“competitor”), the indicated mutants thereof or of an oligonucleotide containing an E-box sequence from the *Ubap2*-promoter. Supershift assays were performed using α-Miz1 (H190, G18, C19), α-Myc (N262), or control antibodies. * designates a non-specific band. The sequences of the oligonucleotides used are shown above the panel; mutated nucleotides are shown in bold.

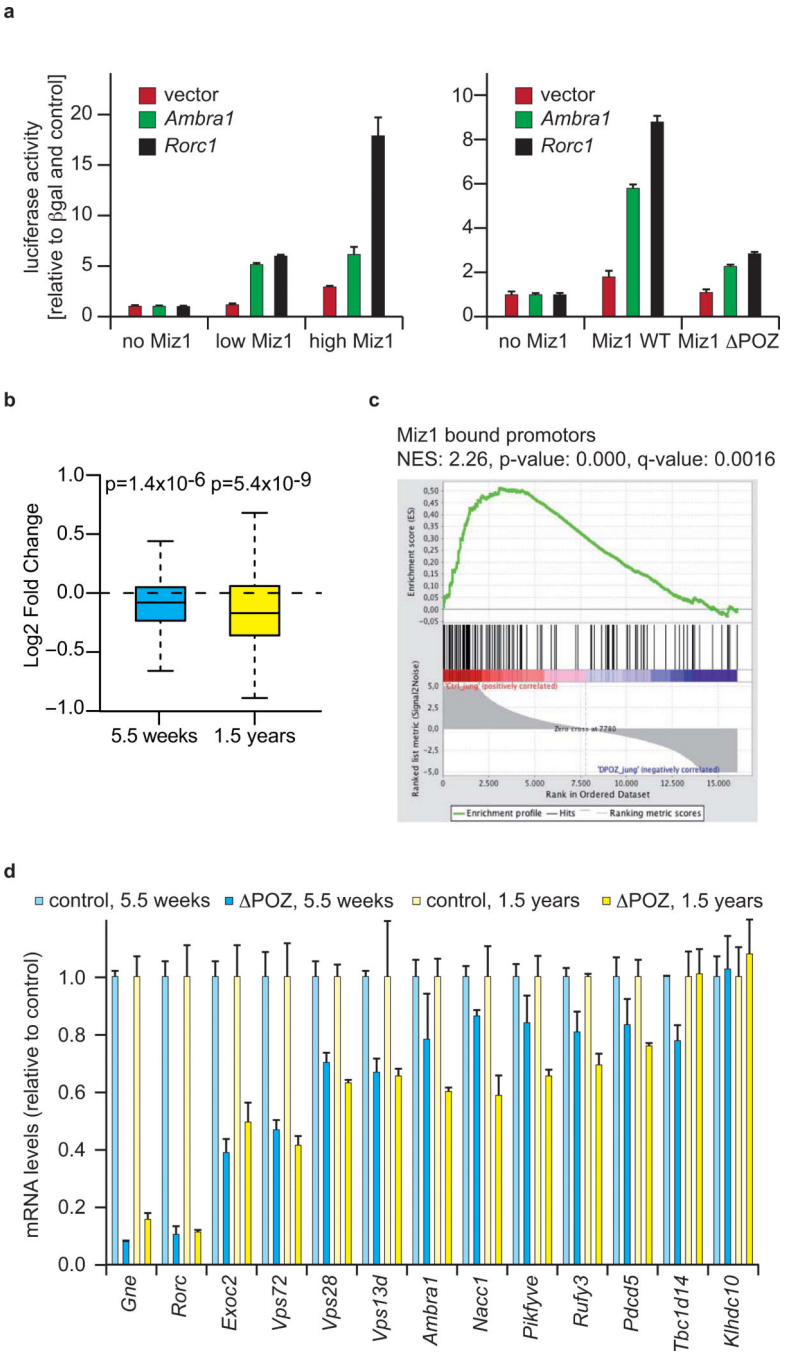

Figure 4. Miz1 is a transcriptional activator of genes involved in vesicular transport

(a) Miz1 activates the *Rorc* and *Ambra1* promoters and the POZ domain is required for activation. HEK293 cells were transiently transfected with plasmids containing promoter sequences of *Ambra1* or *Rorc* in front of luciferase and with expression vectors encoding Miz1 or Miz$^{\Delta POZ}$. Empty vectors were used as control. Values were normalized with CMV-βGal. Error bars are standard deviation (SD) of biological triplicates.

(b) Direct target genes of Miz1 are downregulated in cerebella of *Miz1*$^{\Delta POZNes}$ mice. Microarray analysis was performed from cerebella of mice at the indicated ages. The panels

show box plots of relative gene expression (plotted as $\log_2$ fold change) of the 140 Miz1 direct target genes comparing control and *Miz1*$^{\Delta POZNes}$ mice. The p-value was calculated using a Mann–Whitney–Wilcoxon-test. Microarrays were performed as technical duplicates from RNA pooled from two animals for each genotype.

(c) Gene set enrichment analysis [18] documenting significant downregulation of Miz1 target genes in cerebella of Miz1$^{\Delta POZNes}$ mice. NES: normalized enrichment score (*NES*). Target genes of Miz1 were the only significant gene set in this analysis.

(d) qRT-PCR documenting expression of selected Miz1 target genes in cerebella of control and of *Miz1*$^{\Delta POZNes}$ mice at the indicated ages. Data represent the mean of two independent biological experiments each with three technical replicates. Error bars are SEM.

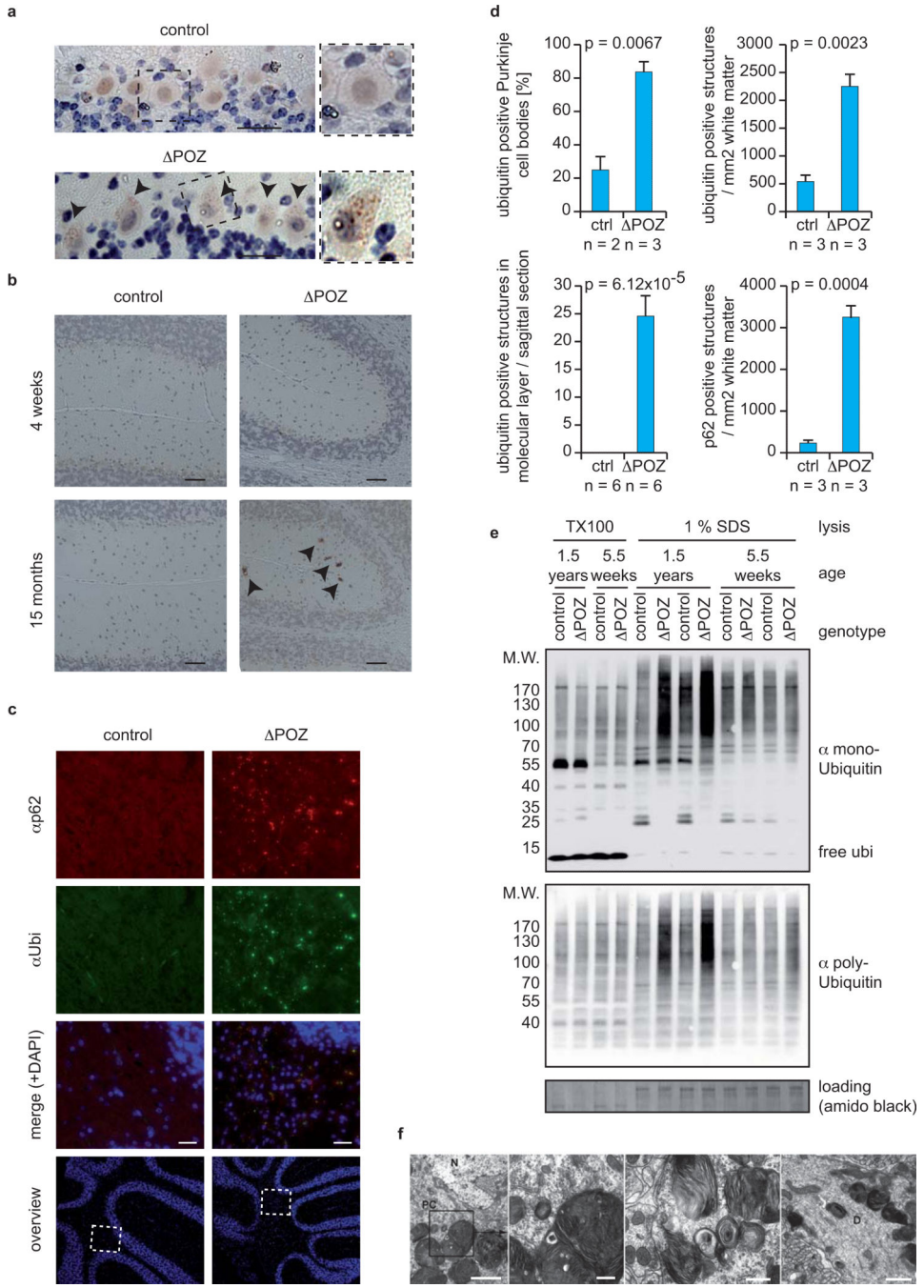

Figure 5. Ubiquitinated proteins and p62/Sqstm1 accumulate in an age-dependent manner in cerebella of *Miz1*$^{\Delta POZNes}$ mice

(a,b) Immunostaining using an α-ubiquitin antibody of (a) Purkinje cells and (b) the molecular layer of *Miz1*$^{\Delta POZNes}$ and age-matched control mice (dotted area: higher magnification). Arrowheads designate ubiquitin-positive structures. Scale bar: (a) 25 μm; (b) 50 μm.

(c) Immunofluorescence staining using an α-p62 and an α-ubiquitin antibody of the white matter of cerebella from *Miz1*$^{\Delta POZNes}$ and age-matched control mice. Nuclei were

counterstained with DAPI and overviews of the cerebella clarifying the selected areas are shown. Scale bar: 25 μm.

(d) Quantification of a, b and c. Error bars represent SEM derived from the indicated numbers of animals. p-values were calculated using an unpaired two-tailed Student's t-test.

(e) Immunoblots of Triton X-100 soluble ("TX100") and insoluble ("1% SDS") fractions of cerebella obtained from control and *Miz1*$^{\Delta POZNes}$ mice of the indicated ages. Blots were probed with antibodies recognizing either mono- or polyubiquitinated proteins. Staining of the membrane with amido black was used as loading control.

(f) Transmission electron microscopy documenting the accumulation of large multilamellar bodies in Purkinje cell bodies (PC) and Purkinje dendrites (D) of *Miz1*$^{\Delta POZNes}$ mice (N: nucleus). Such structures were not observed in age-matched control mice (as quantified in Supplementary Figure S7b). Mean age of mice for all electron microscopy pictures is 13 months for *Miz1*$^{\Delta POZNes}$ and 12.5 months for control mice. Morphologically similar structures accumulate in neurons of mice deficient in late steps of autophagy [28]. Scale bars: 2, 0.2, 0.5 and 1 μm, respectively.

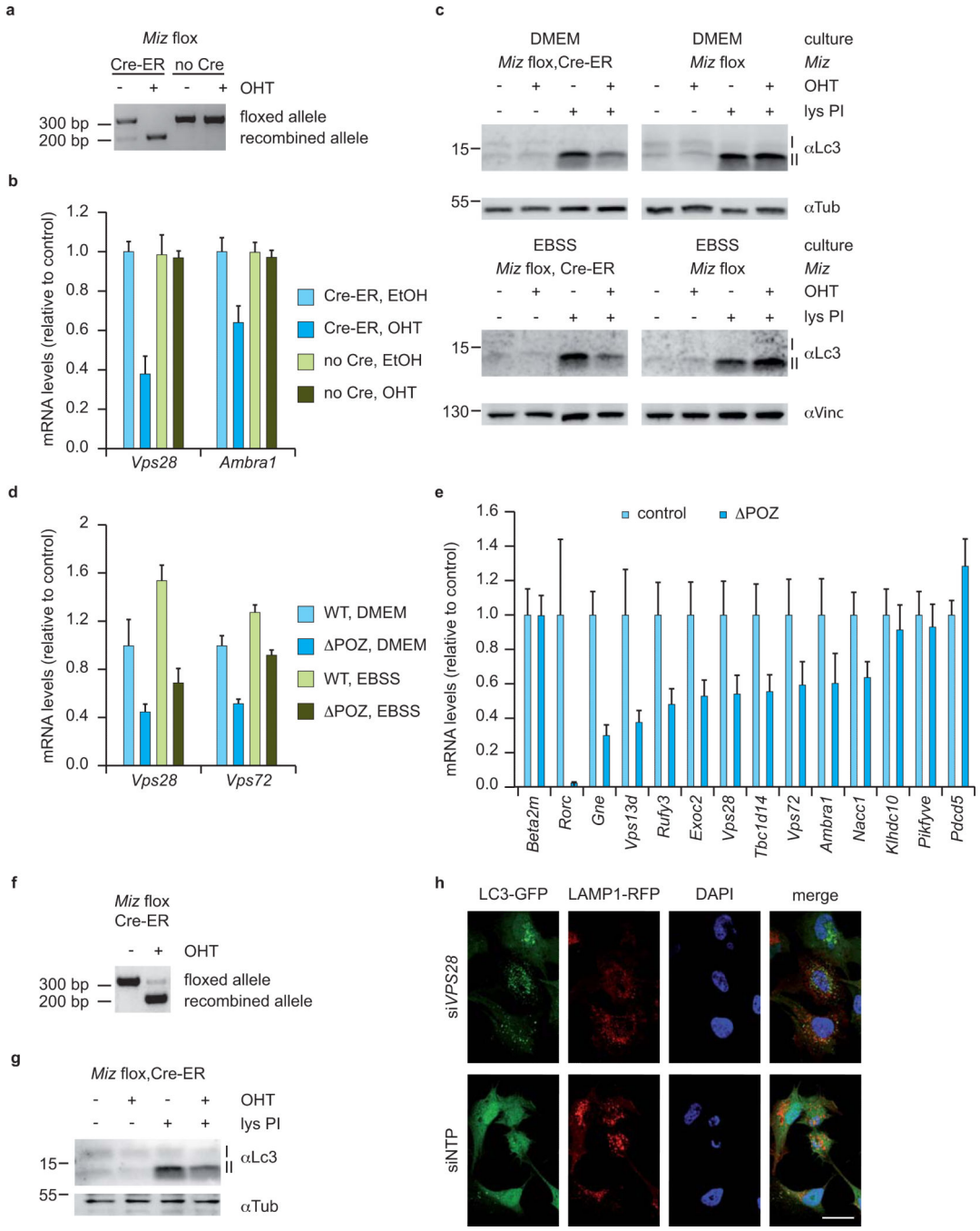

Figure 6. Miz1 is required for maintaining autophagic flux

(a) Genomic PCR documenting recombination of the floxed *Miz1* alleles in Cre-ER positive and negative MEFs. 4-OHT was added to the media for 4 days.

(b) qRT-PCR assays of Miz1 target genes in *Miz1*$^{flox/flox}$Cre-ER^{-} and *Miz1*$^{flox/flox}$Cre-ER^{+} MEFs. The experiment was performed independently from four embryos with identical results. Error bars depict SD of technical triplicates from one experiment.

(c) Immunoblots using an $\tilde{\alpha}Lc3$ antibody detecting Lc3-I and conjugated Lc3-II. 4-OHT-treated and control-treated MEFs of the indicated genotype were incubated with leupeptin

and ammonium chloride (lys PI) for two hours in DMEM (+ amino acids) or in EBSS (- amino acids) medium. The expression of α-tubulin (upper panels) or α-vinculin (lower panels) was used as loading control.

(d) qRT-PCRs of Miz1 target genes in control and *Miz1*$^{\Delta POZ}$ MEFs after incubation in DMEM or in EBSS. Error bars depict SD of technical triplicates from one experiment.

(e) qRT-PCR assays documenting expression of the indicated Miz1 target genes in control and *Miz1*$^{\Delta POZ}$ neurospheres; assays were performed at passage three. SEM values are derived from six biological replicates, each with technical triplicates.

(f) Recombination of *Miz1*$^{flox/flox}$Cre-ER^{+} neurospheres was tested by genomic PCR. 4-OHT was added to the media for three days.

(g) Immunoblots using an α-Lc3 antibody detecting Lc3-I and Lc3-II. 4-OHT treated and non-treated *Miz1*$^{flox/flox}$Cre-ER^{+} neurospheres were incubated with leupeptin and ammonium chloride (lys PI) for 30 minutes. The expression of α-tubulin was used as loading control.

(h) Fluorescent microscopy of SHEP cells stably infected with lentiviruses expressing Lc3-GFP and Lamp1-RFP (to mark lysosomes). *Vps28* was depleted with siRNAs and a non-targeting pool (siNTP) was used as a control. Note the accumulation of Lc3 in vesicles that do not overlap with lysosomes upon depletion of Vps28. Scale bar: 25 μm.

Table 1

Functional annotation of selected Miz1 target genes. Microarray results of the listed genes show the comparison of cerebella samples between old control and *Miz1*$^{\Delta POZNes}$ mice. A (+) in the column Miz1 bound promoters indicates that Miz1 binding was detected in the ChIP-Seq experiment. See Supplementary Table S3 for all microarray results of the listed genes, additional functional annotation, and full references.

Gene symbol	gene name	control/ΔPOZ [logFC]	Miz1 bound promoter	documented role in vesicular transport	documented role in autophagy
Rorc	RAR-related orphan receptor gamma	−2.70	+	+	+
Gne	glucosamine (UDP-N-acetyl)-2-epimerase/N-acetylmannosamine kinase	−1.70	+		+
Trpml1	mucolipin 1	−1.34		+	+
Vps72	vacuolar protein sorting 72	−0.64	+	+	
Vps13d	vacuolar protein sorting 13 D	−0.62	+	+	
Mlst8	MTOR associated protein, LST8 homolog	−0.60	+		+
Pikfyve	phosphoinositide kinase, FYVE finger containing	−0.58	+	+	+
Rufy3	RUN and FYVE domain containing 3	−0.55	+	+	+
Exoc2	exocyst complex component 2	−0.50	+	+	+
Ambra1	autophagy/beclin 1 regulator 1	−0.49	+		+
Nacc1	nucleus accumbens associated 1, BEN and BTB (POZ) domain containing	−0.49	+		+
Vps28	vacuolar protein sorting 28	−0.38	+	+	+
Klhdc10	kelch domain containing 10	−0.19	+		+
Tbc1d14	TBC1 domain family, member 14	−0.07	+	+	+
Pdcd5	programmed cell death 5	−0.04	+		+
Vamp4	vesicle-associated membrane protein 4	−0.03	+	+	+
Pex14	peroxisomal biogenesis factor 14	0.00	+	+	+